Available at www.ComputerScienceWeb.com
POWERED BY SCIENCE DIRECT®

Medical Image Analysis 7 (2003) 207–220

MEDICAL IMAGE ANALYSIS

www.elsevier.com/locate/media

Statistical shape analysis of neuroanatomical structures based on medial models

M. Styner[a,*], G. Gerig[a,b], J. Lieberman[b], D. Jones[c], D. Weinberger[c]

[a]*Department of Computer Science, University of North Carolina, Chapel Hill, NC 27599, USA*
[b]*Department of Psychiatry, University of North Carolina, Chapel Hill, NC 27599, USA*
[c]*National Institute of Mental Health, Clinical Brain Disorders Branch, Bethesda, MD, USA*

Received 4 October 2001; received in revised form 2 May 2002; accepted 20 September 2002

Abstract

Knowledge about the biological variability of anatomical objects is essential for statistical shape analysis and discrimination between healthy and pathological structures. This paper describes a novel approach that incorporates the variability of an object population into the generation of a characteristic 3D shape model. The proposed shape representation is a coarse-scale sampled medial description derived from a fine-scale spherical harmonics (SPHARM) boundary description. This medial description is composed of a net of medial samples (m-rep) with fixed graph properties. The medial model is computed automatically from a predefined shape space using pruned 3D Voronoi skeletons. A new method determines the stable medial branching topology from the shape space. An intrinsic coordinate system and an implicit correspondence between shapes is defined on the medial manifold. Several studies of biological structures clearly demonstrate that the novel representation has the promise to describe shape changes in a natural and intuitive way. A new medial shape similarity study of group differences between monozygotic and dizygotic twins in lateral ventricle shape demonstrates the meaningful and powerful representation of local and global form.

Keywords: Medical image analysis; Shape analysis; Voronoi skeleton; Medial shape description; Brain morphometry

1. Introduction

Quantitative morphologic assessment of individual brain structures in neuroimaging most often includes segmentation followed by volume measurements. Volume changes are intuitive features as they might explain atrophy or dilation of structures due to illness. On the other hand, structural changes like bending/flattening or changes focused at a specific location of a structure, for example thickening of the occipital horn of ventricles, are not sufficiently reflected in global volume measurements. The development of new methods for three-dimensional shape analysis incorporating information about statistical biological variability aims at tackling this issue. In this paper, we present a novel framework for building 3D shape models based on a medial representation to be used for statistical shape analysis of anatomical structures. As shown in this paper, a medial shape representation differs significantly from alternative shape characterization techniques described below.

One of the first to mathematically analyze shape changes was D'Arcy Thomson (Thomson, 1942) in his ground breaking book *On Growth and Form*. Most of the shape analysis are heavily influenced by D'Arcy's work. Bookstein (1997) and Dryden and Mardia (1993) were some of the first to develop mathematical methods to analyze 3D shape based on sampled boundary descriptions.

Davatzikos et al. (1996) proposed an analysis of shape morphometry via a spatially normalizing elastic transformation. Inter-subject comparisons were made by comparing the individual transformations. The method is

*Corresponding author. Tel.: +1-919-962-1919.
E-mail address: martin_styner@ieee.org (M. Styner).

1361-8415/03/$ – see front matter
doi:10.1016/S1361-8415(02)00110-X

applied in 2D to a population of corpora callosa. A similar approach in 3D has been chosen by Joshi et al. (1997) to compare hippocampi. Using the viscous fluid transformation proposed by Miller (Christensen et al., 1994), inter-subject comparisons were made by analyzing the transformation fields. The analysis of transformation fields in both methods has to cope with the high dimensionality of the transformation and the sensitivity to the initial position. Although the number of subjects in the studied populations is low, both show a relatively stable extraction of shape changes (Csernansky et al., 1998). Thompson and co-workers (2000a,b) also use a non-rigid transformation to detect sulcal variability and morphological changes in normal brain development and in disease specific progression. The analysis of shape using point distribution models (PDM) and their deformations was investigated by Cootes et al. (1995).

The approach taken by Kelemen et al. (1999) evaluates a population of 3D hippocampal shapes based on a boundary description by spherical harmonic basis functions (SPHARM), which was originally proposed in (Brechbühler et al., 1995). The SPHARM shape description delivers a correspondence between shapes on the boundary, which is used in the statistical analysis. As in the approaches discussed before, this approach has to handle the problem of high dimensional features versus a low number of samples. Furthermore, the detected shape changes are expressed as changes of coefficients that are hard to interpret.

Golland et al. (1999) in 2D and Pizer et al. (1999) in 3D proposed two different approaches of applying shape analysis to a medial shape description. In his seminal work, Blum (1967) claims that medial descriptions are based on the idea of a biological growth model and a 'natural geometry for biological shape'. The medial axis in 2D captures shape intuitively and can be related to human vision (Burbeck et al., 1996; Siddiqi et al., 1997). Both Pizer and Golland propose a sampled medial model that is fitted to individual objects. By holding the topology of the model fixed, an implicit correspondence between objects is given and statistical shape analysis can directly be applied.

Giblin and Kimia (2000) proposed a medial hypergraph in 3D. They showed that the hypergraph completely characterizes the shape of an object. Similar to work in 2D by Siddiqi et al. (1999), this hypergraph could be used for shape recognition and shape design. To our knowledge, no studies have been done towards using the medial graph/hypergraph directly for shape analysis.

In this paper we present a new approach to shape analysis using medial descriptions. The medial description is computed automatically from a population of objects described by their boundaries. The topology of the medial description is calculated by studying the topological changes of pruned 3D Voronoi skeletons. Voronoi skeletons as shape representations have been studied intensively in past. The most influential pruning related studies in regard to this work have been performed by Ogniewicz and Ilg (1992), Näf et al. (1996) and Attali et al. (1997).

This paper is organized as follows. In the next section, the motivation of our work is presented guided by an example that illustrates the advantages of using medial descriptions for shape analysis. Then, we discuss our methods to generate a stable sampled medial description automatically from a population of objects. We start with a general description of the scheme and discuss shape space, common medial branching topology and minimal sampling in detail. In the result section, several neuroimaging applications of medial shape analysis are presented.

2. Motivation: shape analysis in an example asymmetry study

This section illustrates our motivation to use medial descriptions for shape analysis. A single example is presented from which no conclusions in regard to clinical validity should be drawn, but it illustrates the intuitive understanding and local aspects of shape changes computed with medial descriptions. The presented thickness analysis cannot be done in such fashion using boundary descriptions. Details of the sampled medial description are omitted in this section and described later.

The example is an analysis of left/right asymmetry in a single hippocampus, a subcortical human brain structure which is of interest in neuro-imaging research of schizophrenia, epilepsy and Alzheimer's disease. Asymmetry is defined via the interhemispheric plane, therefore the right hippocampus was mirrored at this plane for comparison. The hippocampi were segmented from a IRprepped SPGR MRI dataset of a normal control subject as part of a large study on hippocampal volume and shape difference in Schizophrenia (Gerig et al., 2002; Schobel et al., 2001). The segmentation is done via a manual outlining procedure based on a strict protocol performed by a clinical expert. The main advantage of medial descriptions is the decoupling of the local shape properties thickness and position, encoded in the properties of the medial axis. In the presented case we chose to focus on the thickness information of the medial manifold.

Fig. 1 displays the surface and medial description of the left and right hippocampal structures, clearly illustrating asymmetry. Volume and medial axis length measurements indicate the same result that the right hippocampus is larger than the left: $\text{vol}_{\text{right}}=2184$ mm^3, $\text{vol}_{\text{left}}=2023$ mm^3; $\text{axis}_{\text{right}}=65.7$ mm, $\text{axis}_{\text{left}}=64.5$ mm. But these measurements do not provide a localization of the detected asymmetry. However, this asymmetry can easily be computed and intuitively visualized using our medial description.

Analysis of the thickness of the hippocampi along the medial axis (the intrinsic coordinate system) reveals a more localized understanding of the asymmetry. In Fig. 2

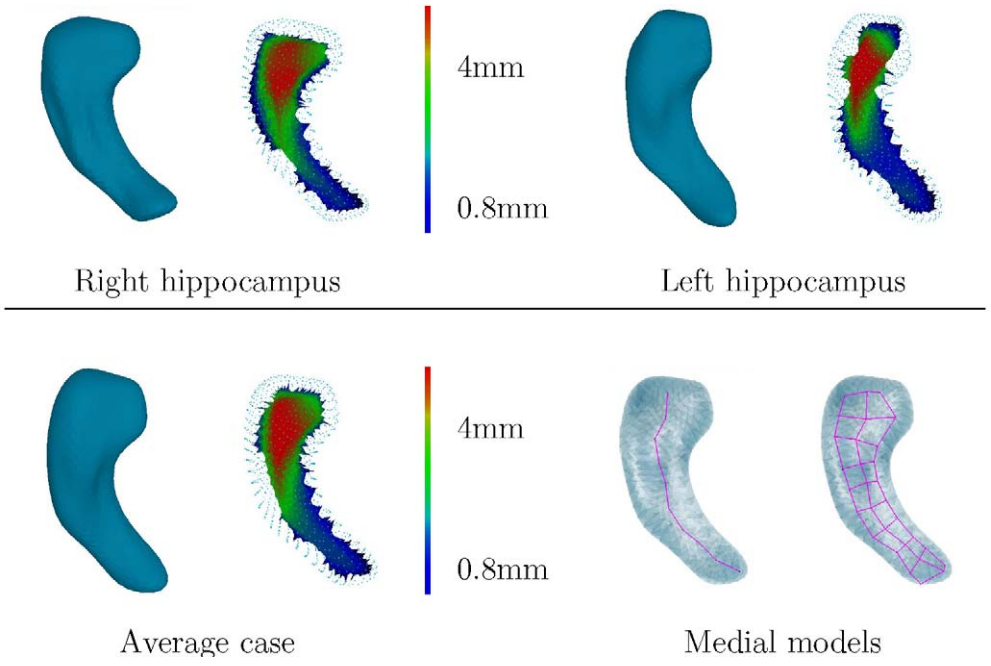

Fig. 1. Visualization of a left/right hippocampus pair with its average structure. Boundary description (left), pruned Voronoi skeleton (right) with thickness coloring (same range for all objects). The figure on the lower right shows the medial axis and medial grid of the average structure.

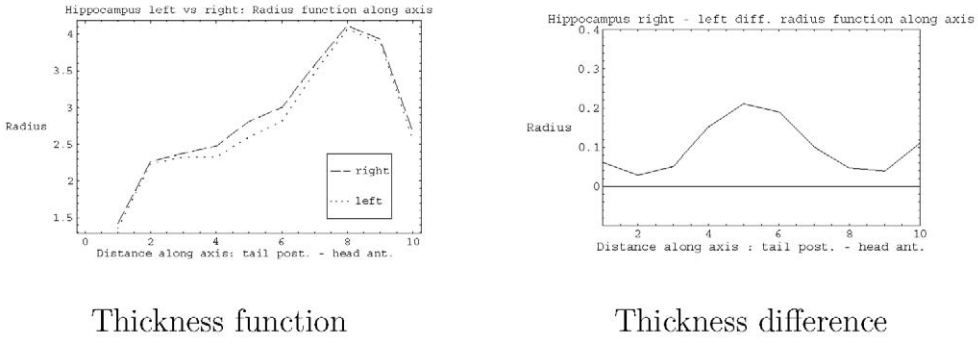

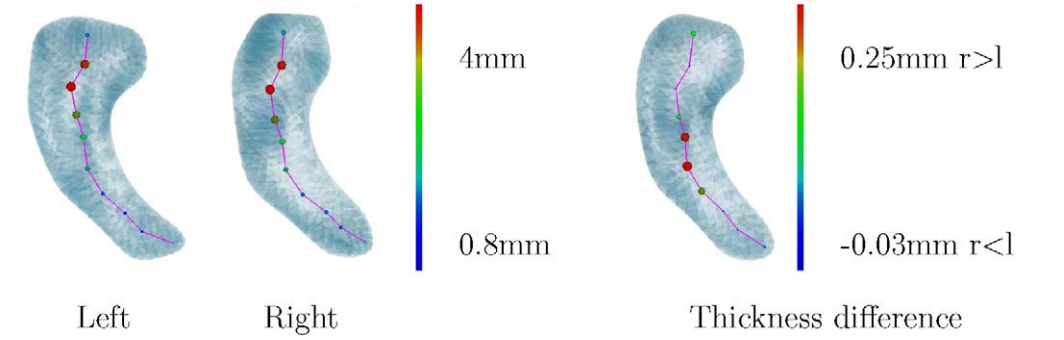

Fig. 2. Thickness asymmetry along medial axis (tail to head). Top row: thickness plot and thickness difference plot. Thickness difference shows $r_R - r_L$. Bottom row: m-rep descriptions with thickness difference $(R - L)$ shown at medial atoms with radius/color proportional to thickness: $r \sim |R - L|$; col $\sim (R - L)$.

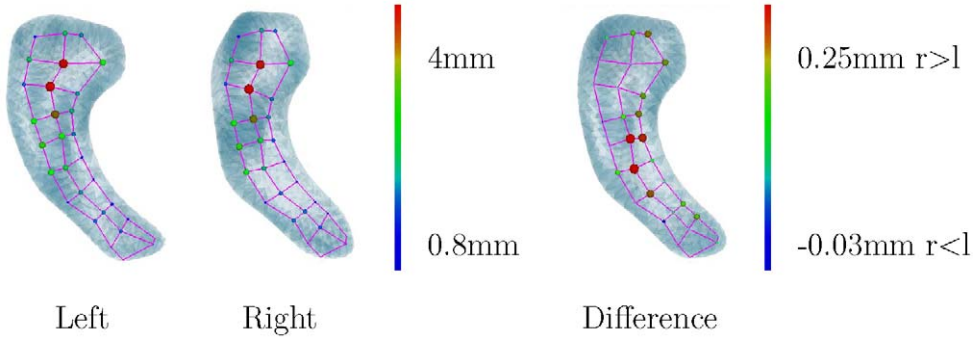

Fig. 3. Thickness asymmetry for a left/right hippocampus pair. Left: m-rep descriptions with radius/color proportional to the corresponding thickness. Right: thickness difference $(R - L)$ at medial atoms with proportional radius/color: $r \sim |R - L|$; $\mathrm{col} \sim (R - L)$.

the right hippocampus is thicker over the full length of the axis, and the difference is most pronounced in the middle part of the axis. In order to relate this thickness information to the appropriate location, we visualize it in the medial samples themselves. Each medial atom (sample of the medial surface) is displayed by a sphere of size and color that is proportional to its thickness. This kind of display can also be used to visualize the thickness difference of corresponding locations in the right and left hippocampus. The sphere radius and color is proportional to the difference: $r \sim |R - L|$; $\mathrm{col} \sim (R - L)$ (see Fig. 2).

As a next step, we take into account a grid of medial atoms and perform the same analysis as for the axis (see Fig. 3). We observe that the right object is thicker, but the difference is most pronounced in the middle part.

In this hippocampus study the medial description gives a better understanding of the observed asymmetry than simple measurements like volume or even the length of the medial axis.

All parts of the processing are described in the methods section. The medial branching topology of one single sheet is computed with volumetric overlap larger than 98% and approximation error E_{pop} less than 0.05.

3. Model building methods

The main problem for a medial shape analysis is the computation of a stable medial model in the presence of biological shape variability. Furthermore, skeletonization procedures are well-known to be very sensitive to small boundary perturbations. Given a population of similar objects, how can we automatically compute a stable medial model? The following sections describe the scheme that we developed to construct a medial m-rep model from a population of objects described by boundary parameterization using spherical harmonics (SPHARM). More details of the model generation can be found in (Styner and Gerig, 2002). There, we also present a stability analysis investigating the influence of shape changes in the object population to the computed medial model.

In overview, our scheme is subdivided into three steps as visualized in Fig. 4. We first define a shape space using principal component analysis of parametrized boundary models. From this shape space we generate the medial model in two steps. First we compute the common branching topology using pruned Voronoi skeletons. Then we compute the minimal sampling of the m-rep model given a maximal approximation error in the shape space.

M-rep models. A m-rep (Pizer et al., 1999) is a linked set of medial primitives called medial atoms, $m = (x;r;\underline{F};\theta)$. The atoms are formed from two equal length vectors and are composed of (1) a position x, (2) a radius r, (3) a frame $\underline{F}$ implying the tangent plane to the medial manifold, and (4) an object angle θ. The medial atoms are grouped into figures connected via interfigural links. These figures are defined as non-branching medial sheets and together form the medial branching topology. The connections of the medial atoms and the figures form a graph called 'medial graph' with edges representing either inter- or intra-figural links.

SPHARM. The SPHARM description is a parametric surface description that can only represent objects of spherical topology (Brechbühler, 1995). The basis functions of the parameterized surface are spherical harmonics. SPHARM can be used to express shape deformations (Kelemen et al., 1999), and is a smooth, accurate fine-scale shape representation, given a sufficiently small approximation error. Based on an uniform icosahedron-subdivision of the spherical parameterization, we obtain a point distribution model (PDM) directly from the coefficients via a linear mapping. Correspondence of SPHARM is determined by normalizing the parameterization to the first order ellipsoid.

3.1. Shape space

As a first step in our scheme, we compute a shape space using principal component analysis (PCA) of SPHARM objects from a training population. The shape space smoothes the individual objects and the shape variability in the training population, thus making the skeleton extrac-

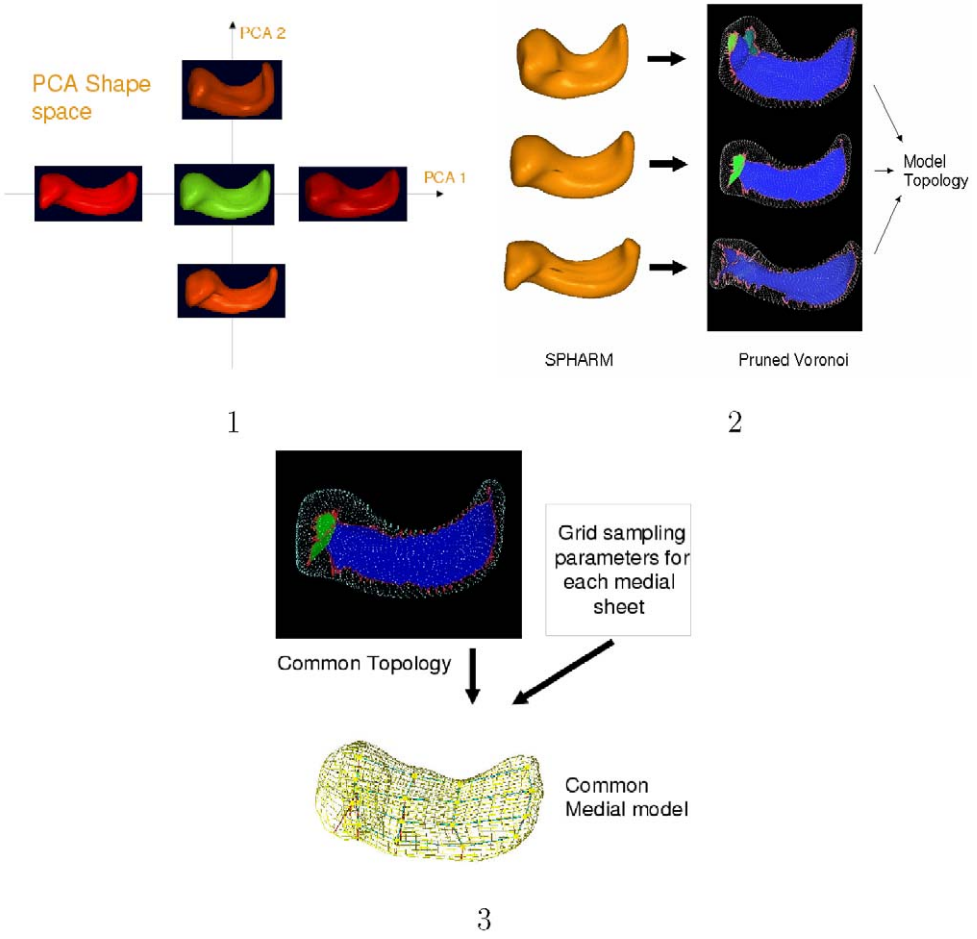

Fig. 4. Computation of an m-rep model from an training population. (1) Shape space definition from training objects. (2) Common medial branching topology as combination of branching topologies from a minimal set of objects in shape space. (3) Minimal sampling of common medial branching topology.

tion and pruning more stable. We assume that the shape space is an appropriate representation of the object's biological variability. PCA is computed from the SPHARM objects as described by Kelemen et al. (1999) resulting in the average coefficient vector and the eigenmodes of deformation. The bases of the shape space are the first eigenmodes that cover at least 95% of the population's variability.

A discrete description of the shape space is obtained by sampling it either uniformly or probabilistically. These samples form an object set that is a representative sampling of the shape space. All subsequent computations of the model building are then applied to this object set.

3.2. Computing a common medial branching topology

Branching topology of a single object. The branching topology for a single object is derived via Voronoi skeletons from finely sampled PDMs. A face-grouping/merging algorithm has been developed that groups the Voronoi faces into a set of non-branching medial sheets. The medial sheets are weighted by their volumetric contribution to the overall object volume: $C_{\text{sheet}} = (\text{vol}_{\text{skel}} - \text{vol}_{\text{skel}\setminus\text{sheet}})/\text{vol}_{\text{skel}}$. The sheets are then pruned using a topology preserving deletion scheme that successively removes non-salient sheets with small volumetric contributions. Fig. 5 illustrates the pruning of the Voronoi skeleton of a lateral ventricle.

Our experiments show that a considerable reduction of the number of medial sheets is possible with sacrificing only little accuracy of the reconstruction. In fact, the pruned skeletons of *all* objects studied so far had a volumetric overlap with the original object of more than 98%.

Computation of a common branching topology. August et al. (1999) and Siddiqi et al. (1999) showed that the 2D medial branching topology is quite unstable, which is even more pronounced in 3D. Thus, in order to be able to robustly compare branching topologies, we developed a matching algorithm that is not based on graph matching but on spatial correspondence.

All objects to be compared are mapped into a common spatial frame by a thin plate splines (TPS) registration based on the boundary correspondence established by the

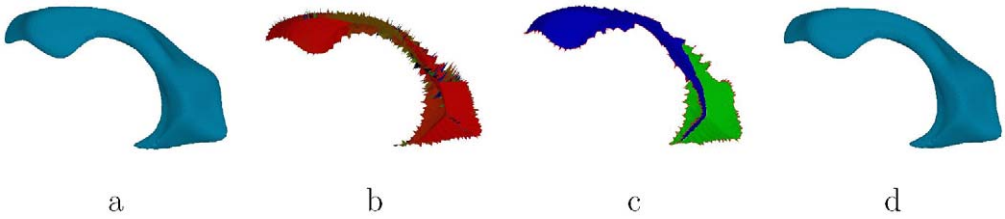

Fig. 5. Voronoi skeleton pruning scheme applied to a lateral ventricles (side views). (a) Original ventricle. (b) Original Voronoi skeleton (~1600 sheets). (d) Pruned skeleton (2 sheets). (c) Reconstruction from pruned skeleton ($E_{\text{overlap}} = 98.3\%$).

SPHARM description. In order to minimize the mapping distortions, the average object of the shape space is chosen to provide the common spatial frame. Individual object skeletons are warped using the TPS interpolation. The common branching topology is then computed iteratively starting with the topology of the average object as the initial guess. The spatial location and shape of each medial sheet is characterized by the center and the second order statistics. Non-corresponding sheets are identified in a one-to-many match procedure using the paired Mahanolobis distance between sheet centers. These non-corresponding sheets are added to the current branching topology. Each sheet of every object in the shape space is matched by at least one sheet in the final common branching topology.

3.3. Minimal sampling of m-rep model

From the common branching topology we compute the sampling of the associated sheets by a grid of medial atoms. The m-rep model is determined by the common branching topology and a set of parameters that specify the grid dimensions for each sheet. The sampling algorithm is based on the longest 1D thinning axis of the edge-smoothed 3D medial sheet. The set of grid parameters is optimized to be minimal while the corresponding m-rep deforms into every object in the shape space with a predefined maximal approximation error. The approximation error is computed as the mean absolute distance (MAD) of the implied and the original boundary. In order to have an error independent of the object size, we normalize with the average radius of all skeletons in the population: $E_{\text{pop}} = \text{MAD}/\text{r}_{\text{avg,pop}}$. Fig. 6 shows the error of various sampling parameters. The limiting error is chosen in the range of 5–10% depending on the structure.

3.4. Deforming the m-rep model into an individual object

This section describes the computation of the m-rep description for shape space objects and individual objects not in the common frame. This computation is done in two steps. An initial estimate is obtained by a TPS warp of the m-rep model from the common frame into the frame of the individual object using the SPHARM correspondence on the boundary. From that position we run an optimization that changes the features of the m-rep atoms to improve the fit to the boundary as described by Joshi et al. (2001). Local similarity transformations as well as rotations of the local angulation are applied to the medial atoms. The fit to the boundary is constrained by a neighborhood dependent prior that guarantees the smoothness of the medial manifold.

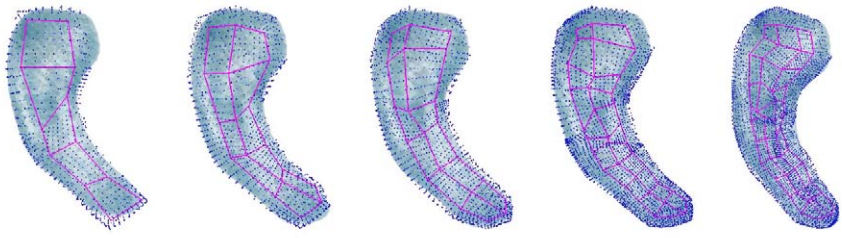

Grid	2x6	3x6	3x7	3x12	4x12
E_{pop}	0.146	0.076	0.075	0.053	0.048

Fig. 6. Sampling approximation errors E_{pop} of the m-rep implied surface (dark blue dots) with the original object boundary (light blue transparent) in a hippocampus structure ($r_{\text{avg}} = 2.67$ mm). The m-rep grids are visualized as red lines. The grid dimensions are shown in the second row, and the E_{pop} errors in the third row.

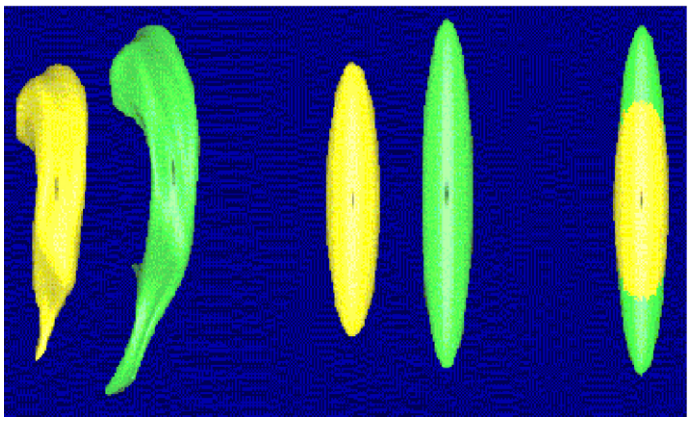

Fig. 7. Object alignment. Two left lateral ventricles are aligned to perfectly match the center and axis of the first order ellipsoid. Left: objects; middle: first order ellipsoids; right: aligned ellipsoids.

4. Object alignment and scaling

As a prerequisite for any shape analysis and shape similarity calculation, objects have to be normalized with respect to a reference coordinate frame. Since we are interested in measuring shape differences, a normalization is needed to eliminate differences that are due to rotation, translation and magnification. Normalization of translation and rotation is accomplished by aligning the objects via the first order ellipsoid (see Fig. 7).

In order to normalize for magnification, an appropriate scaling method has to be defined. The choice of the scaling method depends on the task and the type of objects. There is no clear agreement in literature in regard to which choice is best. We investigated in this paper two possibilities (see also Fig. 8), but there are other valid scaling methods:

(A) No scaling correction: The computation of shape differences without any scale normalization reveals differences between small and large objects even though they might have the same shape properties. Thus, the differences will reflect mixed values of both the shape differences and the size differences.

(B) Uniform scaling to unit volume: Creating a shape difference measure that is orthogonal in its nature to the volume measure has the potential to reveal information additional to size. The volume measurements can be incorporated later into a multivariate statistical analysis as an additional orthogonal feature.

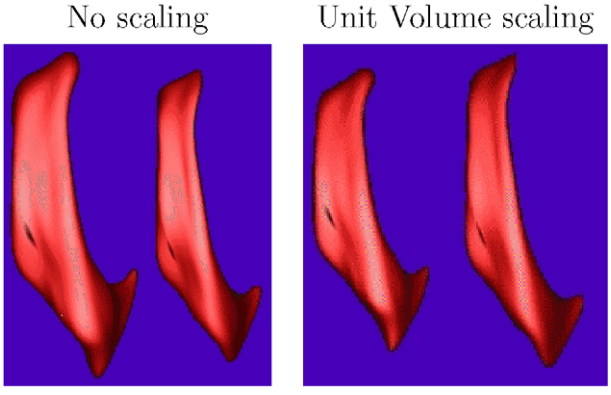

Fig. 8. Object scaling. Pairs of right lateral ventricles (MZ twin pair) unscaled (left) and scaled to unit volume (right). In this example, the scaling procedure corrected for an existing size difference.

5. M-rep shape analysis

The main advantage of a medial shape analysis over a boundary shape analysis is the separate analysis of the two medial shape properties local position and thickness. Fig. 9 demonstrates how thickness and position capture different forms of shape deformation, i.e. thickness changes are due to locally uniform growth forces and positional changes are due to local deformation forces. Since these two features are viewed to be mainly decoupled, we investigate them separately, which provides additional statistical power to our analysis.

When computing group differences instead of pair-wise differences, we designate the average medial description of all groups to be the reference object. Our medial shape analysis computes for each subject the difference to this reference object. In this paper, the presented group study involves pair-wise differences resulting in scalar values, thus there was no need for a reference object.

Using the m-rep description, we can perform a global and a local shape analysis. In the global analysis, we integrate the properties over all atoms of the whole m-rep to compute one position and one thickness feature per m-rep. In the local analysis, we study each atom's properties individually to detect locations of significant differences. In this paper, we treat the atoms to be independent

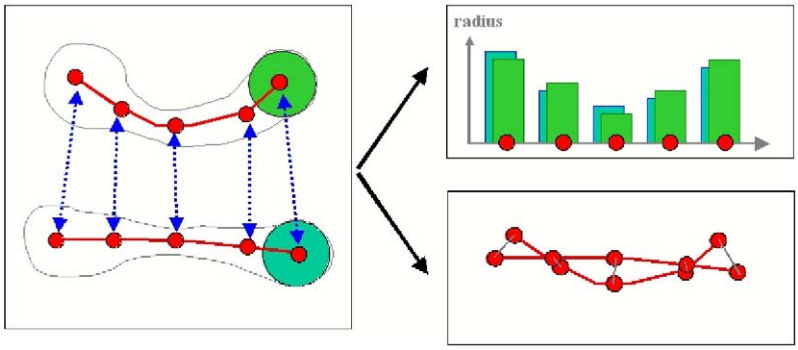

Fig. 9. Medial shape analysis (schematically shown in 2D). The differences in the thickness (radius, top graph) and position properties (lower graph) between two m-reps can be studied separately. The properties express different kinds of underlying processes (growth versus deformation).

of each other. This viewpoint is not fully accurate, but appropriate for a preliminary analysis.

6. Applications

6.1. Medial model computation

The new model building scheme has been applied to different neuroimaging studies with populations of several human brain structures; the overall number of processed cases is shown in parenthesis: hippocampus–amygdala (60 cases), hippocampus (200), thalamus (56), pallide globe (56), putamen (56) and lateral ventricles (80). The computed medial shape models are shown in Figs. 10 and 11. Three of the model building studies are presented in more detail in the following paragraphs.

Hippocampus schizophrenia study. We investigated the hippocampus structure of an object population with schizophrenic patients (56 cases) and healthy controls (26 cases). The goal of this study was to assess shape asymmetry between left and right side objects, and also to analyze shape similarity between patients and controls.

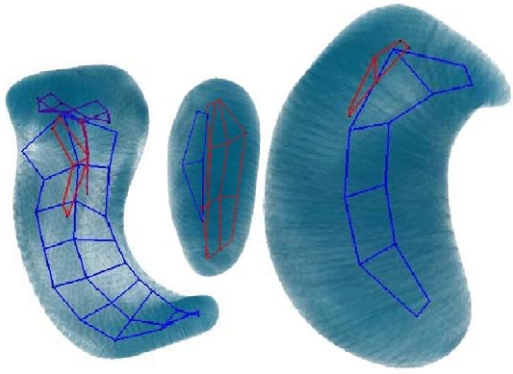

Fig. 11. Medial models of anatomical brain structures. All these models are multi-figure models. From left to right: hippocampus–amygdala complex (4 figures), pallide globe (2 figures) and thalamus (2 figures).

The model was built on a population that included the objects of all subjects on both sides, with the right hippocampi mirrored at the interhemispheric plane prior to the model generation. The hippocampi were segmented from IRprepped SPGR MRI datasets using a manual outlining procedure based on a strict protocol and well accepted anatomical landmarks (Duvernoy, 1998). The

Fig. 10. Medial models of anatomical structures in the left and right brain hemisphere. All these models are single-figure models. From outside to inside: lateral ventricle, hippocampus, pallide globe.

segmentation was performed by a single clinical expert (Gerig et al., 2002; Schobel et al., 2001) with intra-rater variability of the segmented volume measurements at 0.95.

The SPHARM coefficients were normalized for rotation and translation using the first order ellipsoid. The size was normalized to unit volume. The shape space was defined by the first 13 eigenmodes with each of the remaining eigenmodes holding less than 1% of the variability in the population. All objects in the shape space had a medial branching topology of a single medial sheet with a volumetric overlap of more than 98%. Thus, the common topology resulted in a single sheet. The computed minimal grid sampling of 3×8 had an E_{pop} error of less than 5% for all objects in the shape space. The application of this model to the whole hippocampus population of 164 objects generated E_{pop} boundary errors in the range of $[0.048 \ldots 0.088]$ with an average error of 0.058 (see Fig. 12 for a subset of objects). The average radius is 3.0 mm and thus the absolute average error is 0.17 mm. The original sampling is $0.9375^2\times1.5$ mm, which indicates that the individual m-reps are computed with sub-voxel accuracy.

Lateral ventricle twin study. Another study analyzed the lateral ventricle structure in a population of 10 monozygotic and 10 dizygotic twins. Details of the segmentation protocol are described in Section 6.2. The same post-processing has been performed as in the previously described study. The SPHARM coefficients were normalized for rotation and translation using the first order ellipsoid. The size was normalized to unit volume. The first eight eigenmodes defined the shape space, which holds 96% of the variability of the population. The medial branching topologies in the object set varied between one to three medial sheets with a volumetric overlap better than 98% for each object. The single medial sheet topology of the average object matched all sheets in the common frame since the matching algorithm allows one-to-many matches. Thus, the common medial topology resulted in a single sheet. The minimal sampling of the medial topology was computed with a maximal $E_{\text{pop}} \leqslant 0.10$ in the shape space. The application of this model to the whole population generated E_{pop} errors in the range of $[0.057 \ldots 0.15]$ with an average error of 0.094 (see Fig. 13 for a subset of objects). The average radius is 2.26 mm so that the average error becomes 0.21 mm.

Hippocampus–amygdala schizophrenia study. This section presents our scheme applied to a hippocampus–amygdala population from a schizophrenia study (30 subjects). The structures were segmented from SPGR MRI datasets using a manual outlining procedure based on a strict protocol performed by a single clinical expert (Shenton et al., 2002). The segmentations were performed at the Brigham and Women's Hospital, Boston. As in the previously described studies the same post-processing has been applied. The SPHARM coefficients were determined and normalized regarding rotation and translation using the first order ellipsoid. The scale was normalized to unit volume. The shape space is defined by the first six eigenmodes, which cover 97% of the variability in the population. The medial branching topologies in the object set varied between two to five medial sheets with a volumetric overlap of more than 98% for each object. The common branching topology was computed to be composed of four sheets. The minimal sampling of the medial topology was computed with a maximal $E_{\text{pop}} \leqslant 0.10$ in the shape space. The application of this model to the whole population generated E_{pop} errors in the range of $[0.035 \ldots 0.112]$ with an average error of 0.084 (see Fig. 14). The average radius is 3.6 mm and the average error becomes 0.30 mm.

Discussion of model building results. The presented studies of medial model building show that we tested our scheme with anatomical structures of different complexity leading to single and multi figure models. The models are

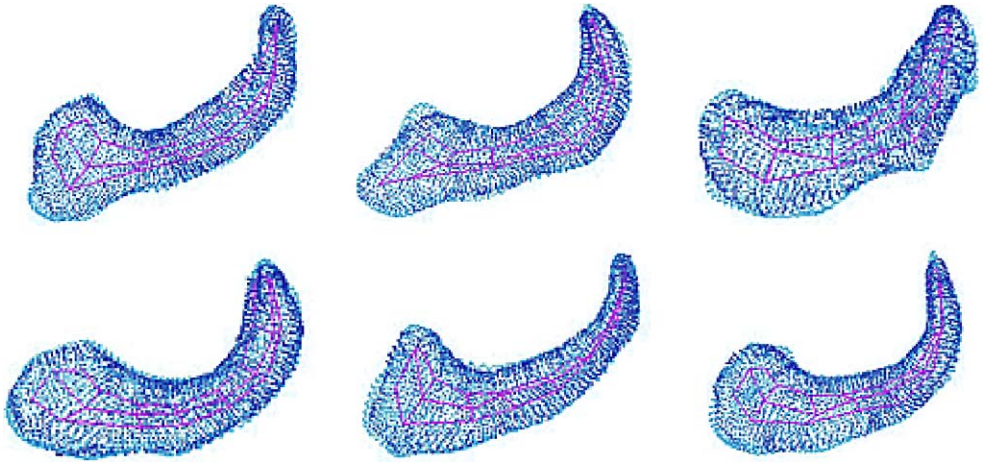

Fig. 12. Six individual m-rep descriptions of the hippocampus study. The visualizations show m-rep grids as red lines, the m-rep implied surface as dark blue dots, and the original object boundary in transparent light blue.

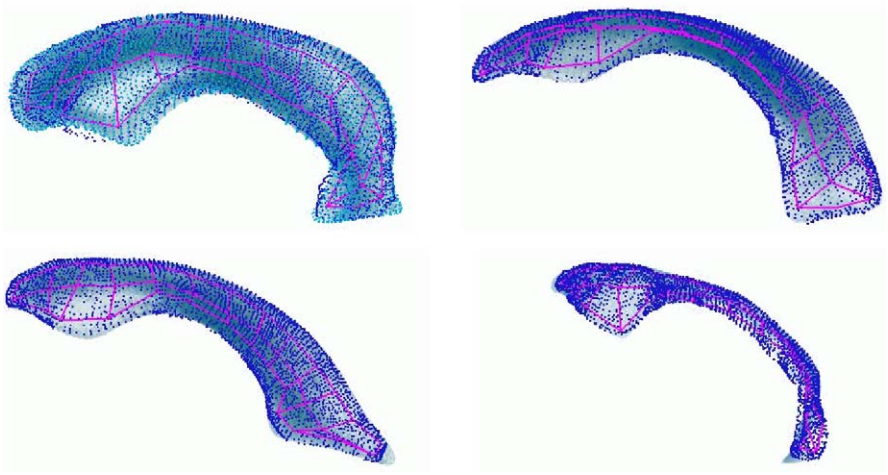

Fig. 13. Four individual m-rep descriptions of the lateral ventricle study. The visualizations show m-rep grids as red lines, the m-rep implied surface as dark blue dots, and the original object boundary in transparent light blue.

computed in a stable fashion and describe individual objects with an appropriately low approximation error. These models can now be used for shape analysis, shape recognition and model based segmentation (Joshi et al., 2001).

In the following section we present an application of a single figure medial model for statistical shape analysis. Multi-figure models can be built reliably, but shape analysis has not yet been performed on such models.

6.2. Shape analysis for group difference

The lateral ventricle study presented before is investigated for group differences between monozygotic (MZ, 5 pairs) twins, dizygotic (DZ, 5 pairs) twins and unrelated (NR, 10 pairs) subjects. All groups are gender, age and handedness matched. The original brain images were provided by D. Weinberger, NIMH Neuroscience in Bethesda, MD, USA. The segmentation method used a single gradient-echo channel (T1w, matrix $256\times256\times128$, resolution $0.9375^2\times1.5$ mm) with manual seeding for Parzen-window based non-parametric supervised statistical classification. Manually guided 3D connectivity was used to extract the left and right lateral ventricles. The segmented structures were postprocessed using a morphological closing operation to provide simply connected 3D objects (see Fig. 15). Minor manual editing was done by a clinical expert to assure the anatomical correctness of all segmentations. The intra-rater variability of this method was measured as 0.97.

In this study, we were mainly interested in investigating the degree of similarity of the lateral ventricles between subject pairs. Thus, the goal of the study was to determine whether MZ twins have more similarly shaped lateral ventricles than DZ twins or unrelated (NR) subject pairs. Knowledge about biological variability and influence by genetic information is essential for any type of morphological neuroimaging study. The population size of each group in this study is very small, so the observed effect must be quite large for the statistical analysis to yield a significant result. A previous study was performed by Bartley et al. (1997) on the same datasets with the goal of distinguishing the groups. They compared cortical gyral patterns and the total brain volumes. Both measures showed significant differences between the MZ and DZ groups.

6.2.1. Volume similarity analysis

We studied each twin pair's similarity using the normalized absolute volume difference: $\Delta\mathrm{vol}_{T_{1,2}}=|\mathrm{vol}_{T_1}-\mathrm{vol}_{T_2}|/(\mathrm{vol}_{T_1}+\mathrm{vol}_{T_2})$. As shown in Fig. 16, there is a trend visible in both brain hemispheres, but no significant conclusions can be drawn since the volume measurement distributions

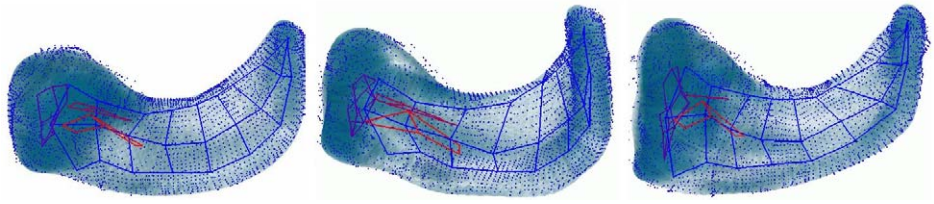

Fig. 14. Three m-rep descriptions of the hippocampus–amygdala study. The visualizations show m-rep grids as colored lines, the m-rep implied surface as dark blue dots, and the original object boundary in transparent light blue.

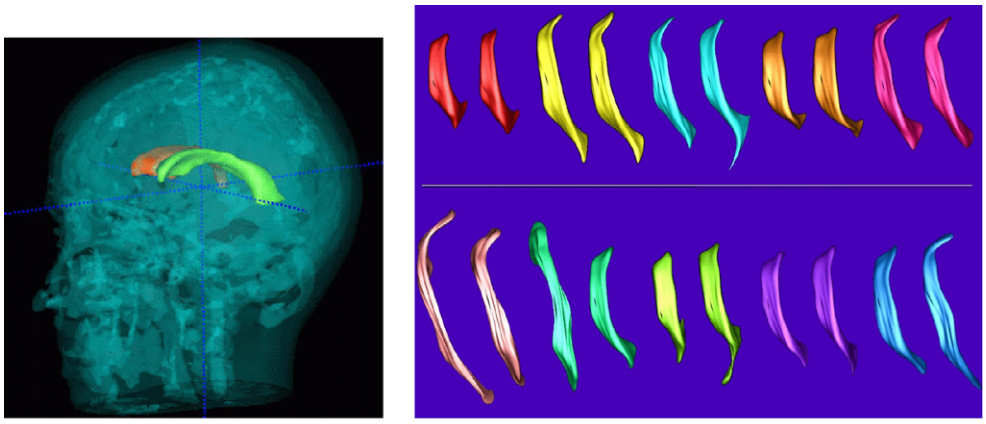

A B

Fig. 15. (A) Three-dimensional rendering of the skin and bone structures of one subject's head (transparent) and the lateral ventricles. (B) Visualization of the right-side lateral ventricles of all twin pairs (same color for pairs) scaled to unit volume. Top row: MZ twins. Bottom row: DZ twins.

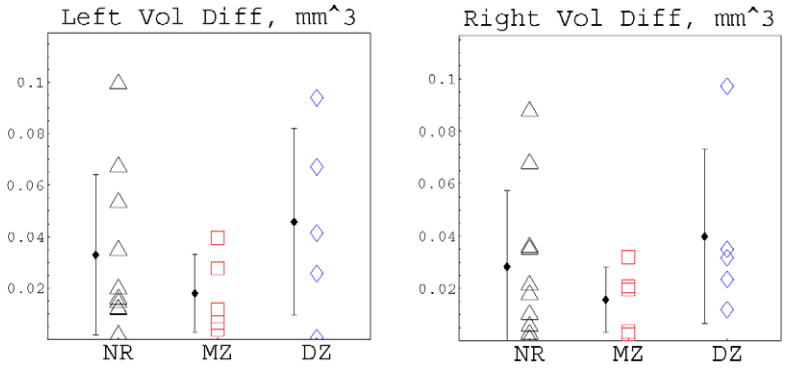

Fig. 16. Plot of pairwise relative volume differences $\Delta \text{vol}_{T_{1,2}}$ between MZ twins (red squares), DZ twins(blue diamonds) twin, and non-related subjects (black triangles). Results of the left and right ventricles are shown in the left and right figures. No significant conclusions can be drawn.

are overlapping. The *P* value for discriminating the two groups is at 0.15/0.16, which is non-significant at a 5% significance level (see Table 1).

6.2.2. Medial shape similarity analysis

Prior to the medial shape analysis, the objects have been normalized to unit volume. The goal of the medial shape analysis was to detect global shape differences and also to pinpoint the locations of significant group difference in a local shape analysis. Eventual differences can manifest in the medial properties of thickness and position (see Section 5), each of them potentially at different locations.

In the global medial shape analysis, we integrate the local differences between corresponding m-rep atoms. The position and the thickness properties display a higher level of similarity between MZ twins than between DZ twins at a significant *p* value (5% significance level) on the right side (see Fig. 17 and Table 1). No significance can be detected on the left side. When studying the joined feature space of both thickness and position differences, this result becomes even more pronounced. Furthermore, when comparing the MZ group to the population of non-related pairs, we observe that the similarity in MZ twins significantly differs from the similarity of non-related pairs. This is not the case for dizygotic twin pairs, thus suggesting that there isn't a difference between DZ and unrelated pairs that can be detected with our methods. We also analyzed the global boundary shape in (Gerig et al., 2001) using the SPHARM description, which had the same outcome as the medial analysis, but with slightly different significance for the test statistics.

Table 1
P values for group mean difference testing between MZ and DZ twin pairs and unrelated pairs

		MZ/DZ	MZ/NR	DZ/NR
Left	Volume diff.	0.151	0.333	0.486
	M-rep global thickness diff.	0.316	0.356	0.959
	M-rep global position diff.	0.157	0.068	0.75
Right	Volume diff.	0.167	0.377	0.500
	M-rep global thickness diff.	0.016[a]	0.011[a]	0.646
	M-rep global position diff.	0.026[a]	0.005[a]	0.91

[a] Indicates numbers that are significant at 5% significance level.

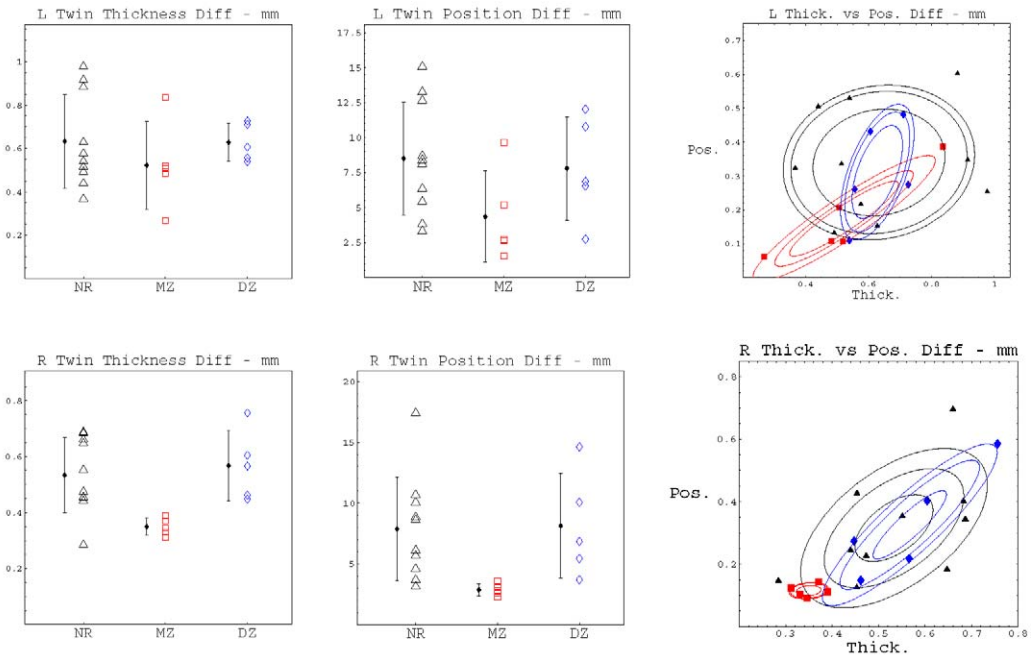

Fig. 17. Plots of pairwise medial shape differences of the thickness (1st column) and position (2nd column) property. In the 3rd column, a combined analysis is shown, which displays the quartile ellipsoids of the three groups (MZ = red squares, DZ = blue diamonds, NR = black triangles). Top row: left ventricle; bottom row: right ventricle. It can be seen that the effect is much stronger for the right ventricle than for the left.

The significant shape differences found with a global shape analysis immediately pose a subsequent research question: Are there subregions that are mainly responsible for similarity/dissimilarity? We used the medial m-rep descriptions to test also for local group differences. The local medial shape analysis is visualized in Fig. 18 by marking locations of significant group differences between MZ and DZ twins. These locations are not the same for the thickness and position features. As in the global analysis, the right ventricle shows a much larger effect than the left

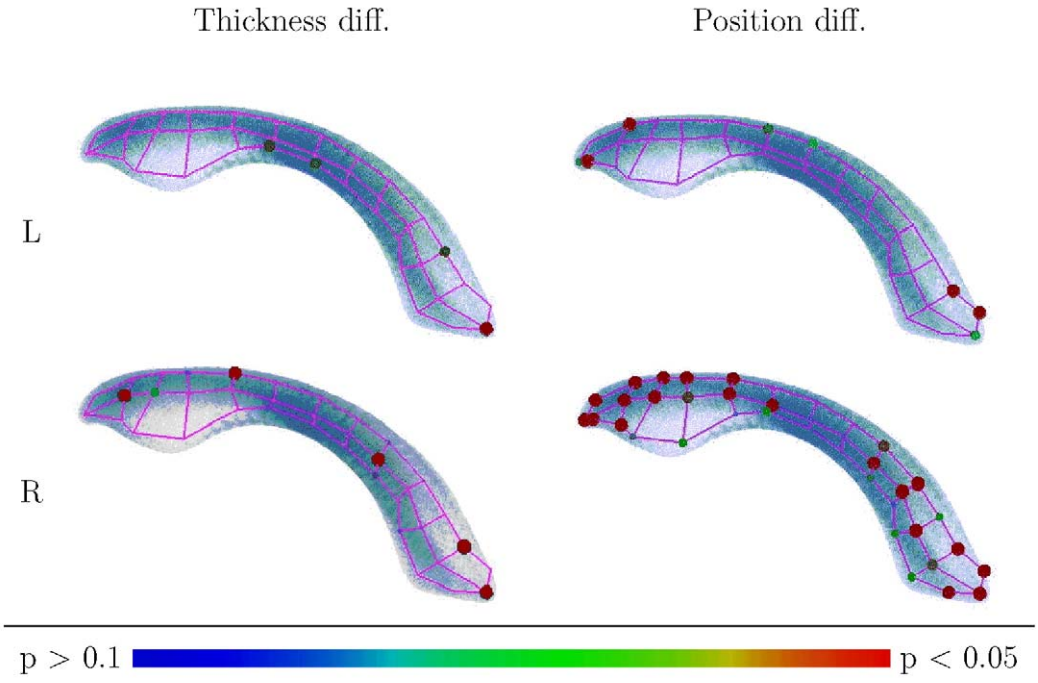

Fig. 18. Local medial shape analysis of MZ versus DZ twin pairs. Lateral ventricles are shown in side view. The radius of the medial atoms is proportional to the significance of the group difference at its location of either the thickness or position property. A clustering in the anterior and posterior part is visible in the right side position analysis (bottom right).

ventricle. It is also clearly visible that the locations of significant difference cluster in the posterior and anterior part regarding the *position* analysis. This suggests that the main shape difference between MZ and DZ twin pairs in this study can be explained in MZ twin pairs having less deformation differences in the posterior and anterior part of the right lateral ventricle than DZ twin pairs.

The results of the medial shape analysis reveals interesting new information about the structure of brain ventricles in genetically identical MZ twin pairs, non-identical DZ twins, and non-related but age and gender matched pairs. We are well aware that we have to be cautious with conclusions due to the small sample size. The size normalized right ventricles reveal that MZ twin pairs present a very small shape difference, with low variability, suggesting that after normalization the objects are indeed very similarly shaped. Surprisingly, this strong and significant effect is not found in the left ventricles, where there is only a trend indicating more similar ventricle shape in MZ as compared to DZ. The statistics further illustrate that DZ twin pairs didn't differ from unrelated pairs using the proposed analysis scheme.

Additionally to the sample size, there is a variety of other factors that influence the results of a shape analysis study like the presented one. The main additional factors include the choice of the segmentation method, the scaling method and the alignment method. The effects of these factors on the shape analysis is part of ongoing research at our laboratory.

7. Summary and conclusions

We present a new approach to description and analysis of shape for 3D objects in the presence of biological variability. The proposed shape description is a medial description derived from a boundary description. The generation of the medial description takes into account the biological variability of a set of training objects, which is a novel concept. We have shown that we can compute a stable medial description for a population of objects. Using the medial description we can visualize and quantitate globally and locally computed shape features regarding similarity. The correspondence given on the medial manifold directly leads to global and local statistical analysis.

The choice of a *fixed* m-rep topology has several advantages, e.g. enabling an implicit correspondence for statistical analysis. On the other hand, a fixed topology m-rep model on a single scale cannot precisely capture the topology of an individual object. The m-rep is therefore always an approximation to the object.

The SPHARM boundary correspondence has shown to be a reliable and robust approach in the general case, but it has inherent problems, e.g. in the case of rotational symmetry. Although not used in our scheme, alternative correspondence methods could be included into the scheme. The investigation of the SPHARM correspondence is ongoing research in our group. We are currently comparing our method with the minimum description length approach of Davies et al. (2002). Also, Meier and Fisher (2002) compared the SPHARM correspondence with an improved method.

The correlation between different medial samples is captured in the medial model, and thus there is the possibility that local effects remain unnoticed in the global analysis. The presented global shape analysis can be enhanced using other measures of global shape difference such as the median values and quantile values. In the presented studies all of these other global measures indicated the same results as the presented ones. It is essential that we are doing additionally to the global analysis, also a local analysis. This is done not just for the localization of effects, but also to capture a real shape difference that might not be captured in the global analysis.

The MZ/DZ twin study demonstrates that shape measures reveal new information additional to size measurements, which might be relevant for improved understanding of structural differences in normal populations but also in comparisons between healthy control groups and patients. Twin studies offer the advantage of reduced natural biological variability by choosing subjects with identical genes. Our twin study demonstrates that significant differences between MZ and DZ pairs could not be found by volume measurements but by shape analysis. There is a significant group difference between MZ and DZ twin pairs for the right but not for the left ventricle. We have no obvious explanation for this finding but hope to get more insight through close collaboration with experts in neurobiology and neurodevelopment. A follow-up study currently analyzes differences between MZ twins discordant for schizophrenia to reveal insight into hypothesized morphologic changes due to illness. Analysis of shape changes similar to the presented case study might become important in longitudinal assessments of morphologic change due to developmental or degenerative processes.

As next steps, we have to study more thoroughly the robustness of our scheme. Furthermore, the local statistical analysis, currently applied independently at each node, needs to take into account local correlation. Additional applications to clinical studies in schizophrenia and other neurological diseases are in progress. Currently we are not using all the properties of the medial representation. The use of the additional information for shape analysis is ongoing research as indicated in (Yushkevich and Pizer, 2001).

Acknowledgements

Miranda Chakos and the neuro-image analysis lab at UNC Chapel Hill, Department of Psychiatry, kindly provided the original MR and segmentations of the hip-

pocampi. Ron Kikinis and Martha Shenton, Brigham and Women's Hospital, Harvard Medical School, Boston provided the original MR and segmentations of the amygdala–hippocampus study. We are thankful to Christian Brechbühler and Gabor Székely for providing the software for SPHARM surface parameterization and description. We are further thankful to Steve Pizer, Tom Fletcher and Sarang Joshi of the MIDAG group at UNC for providing us with m-rep tools. We would like to thank Steve Pizer for his insightful comments and discussions about m-rep and other medial shape descriptions. Sarang Joshi is acknowledged for discussions about the m-rep deformation. Following grants partially funded this work: NCI grant CA 47982, NIH/NIMH funded project Mental Health Clinical Research Center P30-MH33127, and the Foundation of Hope, Raleigh, NC.

References

Attali, D., Sanniti di Baja, G., Thiel, E., 1997. Skeleton simplification through non significant branch removal. Image Processing and Communication 3 (3–4), 63–72.

August, J., Siddiqi, K., Zucker, S.W., 1999. Ligature instabilities in the perceptual organization of shape. Computer Vision and Image Understanding 68, 231–243.

Bartley, A., Jones, D., Weinberger, D., 1997. Genetic variability of human brain size and cortical patterns. Brain 120, 257–269.

Blum, T., 1967. A transformation for extracting new descriptors of shape. In: Models for the Perception of Speech and Visual Form. MIT Press, Cambridge, MA.

Bookstein, F., 1997. Shape and the information in medical images: A decade of the morphometric synthesis. Computer Vision and Image Understanding 66 (2), 97–118.

Brechbühler, C., 1995. Description and Analysis of 3-D Shapes by Parametrization of Closed Surfaces. Dissertation, IKT/BIWI, ETH Zürich, ISBN 3-89649-007-9.

Brechbühler, C., Gerig, G., Kübler, O., 1995. Parametrization of closed surfaces for 3-D shape description. Computer Vision, Graphics, Image Processing: Image Understanding 61, 154–170.

Burbeck, C., Pizer, S., Morse, B., Ariely, D., Zauberman, G., Rolland, J., 1996. Linking object boundaries at scale: a common mechanism for size and shape judgements. Vision Research 36, 361–372.

Christensen, G., Rabbitt, R., Miller, M., 1994. 3D brain mapping using a deformable neuroanatomy. Physics in Medicine and Biology 39, 209–618.

Cootes, T., Taylor, C., Cooper, D., Graham, J., 1995. Active shape models – their training and application. Computer Vision and Image Understanding 61, 38–59.

Csernansky, J., Joshi, S., Wang, L., Haller, J., Gado, M., Miller, J., Grenander, U., Miller, M., 1998. Hippocampal morphometry in schizophrenia via high dimensional brain mapping. Proceedings of the National Academy of Science of USA 95, 11406–11411.

Davatzikos, C., Vaillant, M., Resnick, S., Prince, J., Letovsky, S., Bryan, R., 1996. A computerized method for morphological analysis of the corpus callosum. Journal of Computer Assisted Tomography 20, 88–97.

Davies, R., Twining, C., Cootes, T., Waterton, J., Taylor, C., 2002. A minimum description length approach to statistical shape modeling. IEEE Transactions on Medical Imaging 21 (5), 525–537.

Dryden, I., Mardia, K., 1993. Multivariate shape analysis. Sankhya 55, 460–480.

Duvernoy, H.M., 1998. The Human Hippocampus. Functional Anatomy, Vascularization and Serial Sections with MRI. Springer, Berlin.

Gerig, G., Styner, M., Jones, D., Weinberger, D., Lieberman, J., 2001. Shape analysis of brain ventricles using spharm. In: Mathematical Methods in Biomedical Image Analysis. IEEE CS Press, pp. 171–178.

Gerig, G., Styner, M., Chakos, M., Lieberman, J., 2002. Hippocampal shape alterations in schizophrenia: Results of a new methodology. In: Proceedings of the 11th Biennial Workshop on Schizophrenia, Davos, Abstract.

Giblin, P., Kimia, B., 2000. A formal classification of 3D medial axis points and their local geometry. IEEE Computer Vision and Pattern Recognition, 566–573.

Golland, P., Grimson, W., Kikinis, R., 1999. Statistical shape analysis using fixed topology skeletons: Corpus callosum study. Information Processing in Medical Imaging, 382–388.

Joshi, S., Miller, M., Grenander, U., 1997. On the geometry and shape of brain sub-manifolds. Pattern Recognition and Artificial Intelligence 11, 1317–1343.

Joshi, S., Pizer, S., Fletcher, T., Thall, A., Tracton, G., 2001. Multi-scale deformable model segmentation based on medial description. Information Processing in Medical Imaging, 64–77.

Kelemen, A., Székely, G., Gerig, G., 1999. Elastic model-based segmentation of 3D neuroradiological data sets. IEEE Transactions on Medical Imaging 18, 828–839.

Meier, D., Fisher, E., 2002. Parameter space warping: shape-based correspondence between morphologically different objects. IEEE Transactions on Medical Imaging 21 (1), 31–47.

Näf, M., Kubler, O., Kikinis, R., Shenton, M., Székely, G., 1996. Characterization and recognition of 2D organ shape in medical image analysis using 23 skeletonization. Mathematical Methods in Biomedical Image Analysis, 139–150.

Ogniewicz, R., Ilg, M., 1992. Voronoi skeletons: Theory and applications. IEEE Computer Vision and Pattern Recognition, 63–69.

Pizer, S., Fritsch, D., Yushkevich, P., Johnson, V., Chaney, E., 1999. Segmentation, registration, and measurement of shape variation via image object shape. IEEE Transactions on Medical Imaging 18, 851–865.

Schobel, S., Chakos, M., Gerig, G., Bridges, H., Gu, H., Charles, H., Lieberman, J., 2001. Duration and severity of illness and hippocampal volume in schizophrenia as assessed by 3D-manual segmentation. Schizophrenia Research 49 (1–2), 165.

Shenton, M., Gerig, G., McCarley, R., Székely, G., Kikinis, R., 2002. Amygdala–hippocampus shape differences in schizophrenia: The application of 3D shape models to volumetric MR data. Psychiatric Research Neuroimaging (in press).

Siddiqi, K., Kimia, B., Zucker, S., Tannenbaum, A., 1997. Shape, shocks and wiggles. Image and Vision Computing 17, 365–373.

Siddiqi, K., Ahokoufandeh, A., Dickinson, S., Zucker, S., 1999. Shock graphs and shape matching. International Journal of Computer Vision 1 (35), 13–32.

Styner, M., Gerig, G., 2002. Automatic and robust computation of 3D medial models incorporating object variability. International Journal of Computer Vision (in press).

Thompson, P., Giedd, J., Woods, R., MacDonald, D., Evans, A., Toga, A., 2000a. Growth patterns in the developing brain detected by using continuum mechanical tensor maps. Nature 404, 190–193.

Thompson, P., Mega, M., Toga, A., 2000b. Brain Mapping: The Disorders. Academic Press, New York, Chapter on Disease-Specific Brain Atlases.

Thomson, D., 1942. On Growth and Form, 2nd Edition. Cambridge University Press, Cambridge.

Yushkevich, P., Pizer, S., 2001. Coarse to fine shape analysis via medial models. Information Processing in Medical Imaging, 402–408.